Spatial distribution of potentially toxic element and the potential ecological risk of wolfberry-soil system in genuine producing area of Ningxia，China

Tongning Zhou
Ningxia Medical University
Jiaqi Qin
Ningxia Medical University
Yan Wang
Ningxia Medical University
Yahong Zhang
Ningxia Medical University
Caihong Ma
Ningxia University
Jianjun Yang
Ningxia Medical University
Meilin Zhu (jay70281@163.com)
Ningxia Medical University

Research Article

Keywords: potentially toxic element, wolfberry-soil system, ecological risk, spatial distribution

Posted Date: February 19th, 2021

DOI: https://doi.org/10.21203/rs.3.rs-209472/v1

Spatial distribution of potentially toxic element and the potential ecological risk of wolfberry-soil system in genuine producing area of Ningxia，China

Tongning Zhou[a], Jiaqi Qin[a], Yan Wang[a], Yahong Zhang[b], Caihong Ma[c], Jianjun Yang[a], Meilin Zhu [b, d, *],

[a] College of Public Health and Management, Ningxia Medical University, Yinchuan 750004, China

[b] College of Pharmacy, Ningxia Medical University, Yinchuan 750004, China

[c] College of Resources and Environmental Science, Ningxia University, Yinchuan 750021, China

[d] College of Basic Medical Sciences, Ningxia Medical University, Yinchuan 750004, China

* Corresponding author at, No.1160 Shengli Street, XingQing District, Yinchuan 750004, China.

E-mail address, jay70281@163.com

Abstract

The potentially toxic element (PTE) content and physical and chemical properties of 37 wolfberry and root soil samples obtained from Zhongning county and Shapotou district (Ningxia Hui Autonomous Region) were analyzed, and a potential ecological risk assessment was performed. In addition, multiple linear regression and geostatistical methods were used to predict and analyze the PTE concentrations and potential ecological risks of both soil and wolfberries. The PTE content in the soil was within the standard limits, and only one wolfberry sample contained Cd exceeding the standard limit (by 2.7%). The other potentially toxic elements (PTEs) did not exceed the standard limits. In the regression fitting, the models obtained for Cu, Zn, Pb, and Ni contents in the fruits showed a good correlation ($p < 0.05$), the PTE content of the soil showed an overall trend of high concentrations in the central part of the studied region. The ecological risk of Hg in the soil is rated as high, whereas the risks of the remaining PTEs were mostly medium or low. Further, the predicted PTE content of the wolfberries was generally high in the western region and low in the eastern region, although there were slight variations for different PTEs in some areas.

Keywords potentially toxic element; wolfberry-soil system; ecological risk; spatial distribution

1 Introduction

Since the 1970s, soil pollution has drawn the attention of researchers all over the

world [1-2]. Increasing industrialization, mineral mining, smelting, and atmospheric pollution caused by human activities, as well as long-term sewage irrigation and sludge, chemical fertilizer, and pesticide application to the soil, have resulted in increases in soil pollution [3]. Concerning the pollutants, potentially toxic elements (PTEs) have little mobility in soil and thus generally accumulate in the surface layer. Because this layer is used for animal grazing and crop production, its pollution presents a significant problem, and the study of the contamination of the top layers of soil has attracted significant attention. Crucially, PTEs are easily transferred from the soil to organisms, affecting crop growth and causing food contamination.

Various researchers have investigated the spatial distribution of PTEs using geostatistical technology based on geographic information systems [4-8]. From the perspective of land types, cultivated land, which is intimately associate with human activity, has received significant attention. However, most investigation has focused on common crops, such as wheat and corn [9-10], and their relationship with PTEs in cultivated soil [11], and it has been found that the potentially toxic element (PTE) pollution of certain crops is positively correlated with that of the soil, either directly or by promoting contaminant uptake [12]. Wolfberry (*Lycium barbarum L.*) is a plant belonging to the Lycium genus of the Solanaceae family. Wolfberry typically refers to dried and mature fruits of *L. barbarum* from Ningxia and is the common term for commercial *L. barbarum*, Ningxia *L. barbarum*, Chinese *L. barbarum*, and other *Lycium* species. In recent years, as a result of in-depth research into wolfberry polysaccharides [13-14], Chinese wolfberries have entered the public eye as an important

crop for both medicines and food, and knowledge about their nutritional value has gradually increased [15]. Specifically, wolfberries are rich in vitamins, proteins, minerals, polyphenols, carotenoids, amino acids, and other nutrients, making them an important raw material for the development of nutritional health food products [16]. However, there have been few geographical analyses and predictive studies of the spatial distribution of wolfberries, and there have only been a few studies concerning the PTE pollution and evaluation of the contamination of wolfberries [17-18]. This is crucial because, if the PTE content of the soil used for cultivation is high, wolfberry contamination may occur. Further, although the PTE content of wolfberries is typically reported to be lower than the Chinese standard limits for Chinese medicinal materials, further investigation is required if cultivation and commercialization are to be increased [18].

In this study, the Ni, Cu, Zn, As, Cd, Pb, Cr, and Hg contents of wolfberry fruits and the soil around the roots was investigated. First, the PTE concentration of the soil and potential ecological risks were evaluated, and a spatial prediction of the PTE content was carried out. In addition, because of the discontinuous nature of wolfberry plantations, we used a novel method to predict the contamination of wolfberry fruits via soil contamination, which was assessed using spatial prediction analysis based on geostatistical principles. Specifically, we evaluated the soil system around the roots of the wolfberry plants and explored the correlation and relationship between the soil PTE content and its physicochemical properties (pH, organic matter content, and cation exchange capacity) and the PTE content of wolfberry fruits.

2 Results

2.1 Analysis on the characteristics of PTE content in soil and wolfberries

As shown in Table 1, the average contents of Ni, Cu, Zn, As, Cd, Pb, Cr, and Hg in the soil were 40.95, 5.27, 42.46, 8.36, 0.026, 23, 52.89, and 0.069 mg/kg, respectively. The contents of Ni, Pb, and Hg were slightly higher than the soil background value [19], whereas the contents of Cu, Zn, As, Cd, and Cr were lower than the background value. Crucially, all of these values are lower than the standard limits for these metals [20]. The enrichment ratios were in the order of Hg > Ni > Pb > Cr > Cd > Cu = Zn = As = 0, and the enrichment ratios of Hg, Ni, Pb, Cr, and Cd were 97.3%, 64.86%, 51.35%, 35.14%, and 2.7%. On the basis of the enrichment ratios, the enrichment proportion of Ni, Pb, and Hg is greater than 1, which indicates that these species are accumulated in the soil in this area. The order of the coefficients of variation for these eight elements was Cd > Hg > Pb > Cr > Cu > Ni > As > Zn, ranging from 14.63% to 92.72%. According to Wilding's classification of soil variability based on coefficients of variation, that of Cd, which is greater than 90%, indicates great dispersion and strong variability, i.e., high spatial variability [21], possibly because this element has been disturbed by human activities for a long time. In contrast, the coefficient of variation of Zn is less than 15%, and its degree of dispersion is small, indicating that its spatial variability is weak. Those of the other elements were moderately variable.

The results for the wolfberry samples in the study area are shown in Table 2. Hg was not detected. However, the detection rates of As and Pb were 59.46% and 91.89%, and those of Ni, Cu, Zn, Cd, and Cr were all 100%. The mean contents of Ni, Cu, Zn, As, Cd, Pb, and Cr in the wolfberries were found to be 0.88, 8.7, 19.56, 0.20, 0.10, 0.35,

and 2.62 mg/kg, respectively. The local standard for food safety for Chinese wolfberries (DBS64/001-2017) only contains limits for Pb and Cd: 1.0 and 0.3 mg/kg, respectively. Thus, the Pb contents in the samples are lower than the standard limit. The Cd content in one sample exceeded the standard by 2.7%. The Chinese Pharmacopoeia [22] and "Green standards of medicinal plants and preparations for foreign trade and economy" [23] stipulate the following limits: As ≤ 2 mg/kg, Hg ≤ 0.2 mg/kg, Pb ≤ 5 mg/kg, Cd ≤ 0.3 mg/kg, and Cu ≤ 20 mg/kg. Thus, the Cu, As, and Pb in the wolfberry samples did not exceed the standards. In China, except for those of As, Hg, Pb, Cd, and Cu, national standard limits for the other PTEs Chinese herbal medicines have not established [24].

The mean BCF values for Ni, Cu, Zn, As, Cd, Pb, and Cr in the wolfberries were 0.023, 1.762, 0.475, 0.026, 5.821, 0.017, and 0.056, respectively. The mean BCF of Cd (5.821) was the highest, and that of Pb (0.017) was the lowest. In particular, the BCF values for Cu and Cd are greater than 1, indicating that these elements were highly enriched in the wolfberries. As an organism at a high trophic level, wolfberries contain Cu and Cd concentrations higher than those in the environment, and the contents increase with longer growth and development time.

2.2 Correlation evaluation of the wolfberry–soil system

The Pearson correlation coefficient and statistical significance are shown in Supplementary Table S1 online. There was a significant positive correlation between the Cu content of the wolfberries and the As content in the soil ($p = 0.022$), indicating that the wolfberry plants absorb Cu from the soil ($p < 0.1$). The Pb content in the wolfberries was negatively correlated with Ni and Zn contents in the soil ($p = 0.06$, $p =$

0.093, respectively), which indicates that these metals may play an inhibitory role in the absorption of Pb from the soil. There were no significant correlations between the other PTEs. On adding the physicochemical properties of the root soil (pH, organic matter content, and cation exchange capacity) to the model, the pH was found to be negatively correlated with the Ni, Cu, and Cr contents but positively correlated with As, Cd, and Pb in the wolfberry fruit. The organic matter content and cation exchange capacity in the soil were positively correlated with the PTE content of the wolfberries; in particular, the Cu and Zn contents were positively correlated with the cation exchange capacity ($p = 0.006$ and $p = 0.036$, respectively), which indicates that a high cation exchange capacity promotes the absorption of Cu and Zn by wolfberries.

In this study, a multiple linear regression equation with the PTE content of the wolfberry fruit as the dependent variable and the soil indexes as independent variables was obtained. As shown in Supplementary Table S2 online, when the Cu, Zn, Pb, and Ni contents of the wolfberry fruits were used as dependent variables ($p < 0.05$), the R value for the fits for Cu and Pb were high, indicating a good fit. When the As and Cr contents in wolfberry fruits was used as dependent variables to fit the equation, the p-value slightly exceeded 0.05 ($p = 0.053$). When the Cd content in wolfberry fruits was used as the dependent variable to fit the equation and the level (α) was set to 0.15, no independent variable satisfactorily fit the model. However, only when α was set to 0.2, the soil pH showed correlation (for these parameters, p ranged from 0.186 to > 0.05). In the Pearson correlation analysis, the correlation between the independent and dependent variables was significant ($p = 0.186$), indicating that the multivariate linear

relationship was weak.

2.3 Spatial distribution of soil PTEs and potential ecological risk

Supplementary Table S3 online shows the results of the spatial autocorrelation analysis using ArcGIS 10.0. The Moran's I values for Ni, Cu, Zn, As, Pb, Cr, and Hg in soil are 0.066, -0.148, 0.648, 0.041, 0.337, 0.515, and 0.087, respectively, indicating that all PTEs except Cu show a positive spatial autocorrelation (Moran's I > 0). In particular, the Moran's I of Zn is 0.648, indicating that the Zn content in the soil has a strong positive autocorrelation with the spatial variation and is directly proportional to the degree of spatial aggregation. In contrast, Cu shows a negative spatial autocorrelation (Moran's I < 0), indicating an inverse relationship to the degree of spatial aggregation. In some cases high values are surrounded by low values and low values are surrounded by high values. The *p*-values for Zn, Pb, and Cr are 0 and the Z-scores are all greater than 2.58, indicating that there is a significant spatial correlation. In contrast, the *p*-value of As is 0.396 and the Z-score is less than 1, indicating a weak spatial correlation. Therefore, the As content in the soil is random.

The results of the semivariogram analysis of the seven PTEs in the soil of the wolfberry root system in the study area are shown in Table S4. The semivariogram nuggets (C_0) of the seven PTEs are all greater than 0. $C_0/(C + C_0)$ is the ratio of the spatial variation caused by the random part to the total spatial variability. The ratios of the seven detected PTEs in the root soil samples ranged from 0.012 to 0.276, and that of As was higher than 0.25, indicating that the other six PTEs had a strong spatial correlation. The ratios for Zn, Pb, and Cr are all less than 0.1, which is consistent with

the spatial autocorrelation conclusion given by the Moran's I analysis above, suggesting that that analytical method is reliable. The variogram model type for Ni, Cu, As, and Hg soil contents was Gaussian, whereas the rest were spherical. The R^2 values of each model are between 0.381 and 0.879. Thus, these fit well with the corresponding theoretical model, which helps the Kriging interpolation analysis. The semivariogram ranges of the seven PTEs are between 6870 and 99731.49, which is larger than the sampling distance, thus meeting the requirements for spatial analysis.

Comparing two interpolation graphs (GS+ 10 in Fig. 1 and ArcGIS 10.0 in Fig. 2), we can prove the applicability of the semivariogram fitted by GS+ 10 in ArcGIS 10.0. The 3D inner illustration (Fig. 1) prepared by GS+ 10 shows intuitively the trend for each PTE within the distribution range. Because the plane rectangular coordinate system must be converted when entering coordinates in GS+ 10, the interpolation diagram shows the opposite direction to convention.

In the areal distribution (Fig. 2) based on the GCS-Krasovsky-1940 coordinate system and D-Krasovsky-1940 datum plane, the trends for each PTE in the distribution range are consistent with the 3D inner illustration produced by GS+ 10, which proves the applicability and accuracy of the semivariogram parameters obtained in GS+ 10 for Kriging interpolation and extrapolation in ArcGIS 10.0. Generally speaking, the east–west trend is obvious, whereas the north–south trend is weak. The western region comprises sandy land and mountainous areas, and the contents of Zn, As, and Pb in the soil are relatively low, whereas the contents of Cr, Hg, and Ni are relatively high. In the middle cultivated area, all elements show peaks, indicating that the cultivated land area

has a higher PTE content than those of the mountains and sandy land, most likely because of cultivation, sewage discharge, and fertilizer use, which may all contain PTEs. The highest Cu content is close to the lowest value, indicating that Cu migration in soil is not significant. In contrast, the As content is high, suggesting that attention is required in this area. There is also a relatively high As content in the cultivated land. The eastern and southeastern regions are plain regions and have high values of Ni and Cr, although the Cu content is also high in this region.

Supplementary Table S5 online shows the classification of the potential ecological risk index model for the soil. In the study area, E_{Ni} ranged from 2.734 to 7.813, E_{Cu} ranged from 0.679 to 2.262, E_{Zn} ranged from 0.510 to 0.935, E_{As} ranged from 3.975 to 9.411, E_{Pb} ranged from 3.398 to 12.864, and E_{Cr} ranged from 0.933 to 3.8, E_{Hg} ranged from 21.6 to 482, and E_{total} ranged from 40.704 to 509.238. According to the single risk index, except for Hg, the risk levels of the other six PTEs are all low. For E_{Hg}, there are 1 serious risk level, 9 high risk levels, 24 high risk levels, 2 medium risk levels, and 1 low risk level. According to the overall risk index, there were no points at which E_{total} was rated as heavy or serious risk, although 1 point was rated as high risk, 18 points as medium risk level, and 18 points as low risk. The contribution of each PTE to E_{total} were Ni = 3.33%, Cu = 0.74%, Zn = 0.45%, As = 4.38%, Pb = 3.48%, Cr = 1.10%, and Hg = 86.51%. Except for Hg, the contribution rate of other PTEs is less than 5%, and these six PTEs show no potential ecological risks.

Supplementary Fig. S1 online shows the λ value curve of the Box–Cox normal transformation of E_{total} when λ = 0.3 and $p = 0.097 > 0.05$. The semivariogram fitted

by GS+ 10 has a Gaussian distribution: C_0= 0.264, $C + C_0$= 1.0633, and $C_0/(C + C_0)$= 0.26. However, fitting with ArcGIS 10.0 yielded a stable optimal distribution. After comparing the two interpolation results, the error in the stable distribution was found to be smaller, so it was used for further analysis. Using the GCS-Krasovsky-1940 coordinate system and D-Krasovsky-1940 reference plane, the Kriging interpolation method was used for interpolation prediction analysis for the risks and total risks of seven PTEs. The results are shown in Fig. 3. Six PTEs (Ni, Cu, Zn, As, Pb, and Cr) were assessed as low risk in the whole region, whereas Hg is a high risk, and there are serious risks in the eastern region. On the basis of the E_{total} distribution, the rating of the total risk has declined compared to previous years, and most areas are medium risk, some areas in the middle and southeast regions are low risk, and only a few areas are high risk.

2.4 Spatial distribution characteristics of PTEs concentration of wolfberries based on the soil

Using the linear regression equation in Supplementary Table S2 online, the contents of seven PTEs in wolfberry fruits were calculated. The results of the normality test in Supplementary Table S6 online, show that the data are normally distributed, except for those of As and Cr. After logarithmic transformation, the contents of As and Cr in wolfberries were normally distributed, having $p > 0.05$. On the basis of the data in Supplementary Table S7 online, the proportion of seven PTE elements in the wolfberries is between 0.030 and 0.361, and the Cu, As, Pb, and Cd contents in the wolfberries were higher than 0.25, which indicates that these six PTE contents are

moderately spatially correlated. The Zn, Ni, and Cr contents range from 0 to 0.25, which indicates that there is a strong spatial correlation between the three elements in wolfberries. The variogram model type for Pb, Cd, and Cr contents in wolfberries was Gaussian, that for Cu content was exponential, and those of the other metals were spherical. The R^2 values of each model are between 0.173 and 0.712, and, specifically, the R^2 values of the Cd and Pb models are low. Looking back on the multiple linear regression process, the only independent variable affecting Cd and Pb contents is the pH. Considering the poor spatial correlation of pH values, this may affect the R^2 values of Cd and Pb in wolfberries. However, the other elements fit well under the corresponding theoretical models, which should enable Kriging interpolation analysis. Specifically, in the semivariograms, the range values of the seven PTEs are larger than the sampling distance, between 14690 and 9088070.6, thus meeting the requirements for spatial analysis.

In the analysis of soil PTEs, the applicability of the ArcGIS 10.0 fitted semivariogram was proved by its consistency with the GS+ 10 interpolation and ArcGIS 10.0 expansion distribution, so the expanded Kriging interpolation map could be directly analyzed. Figure 4 shows the results of the Kriging interpolation achieved by importing the parameters of the semivariogram into ArcGIS 10.0. Six of the PTEs in the wolfberry fruits, excluding Cr, generally show a high distributions in the west and a low distribution in the east, having the lowest concentration in the middle region. In contrast, the Cr distribution is smooth, and the first 20% of the concentration range (low concentration) is located east of the middle region, with no high-to-low west-to-

east trend. The concentrations of As, Cd, Ni, and Zn in the wolfberries fall in the first 20% of the concentration range, whereas, for Cr and Cu, this concentration range is distributed over a smaller area. With regard to the PTEs limits for Chinese herbal medicines discussed in Section 3.1, the spatially predicted concentrations of all PTEs did not exceed the standard limits.

3. Discussion

Overall, in the soil, Ni, Pb, and Hg have high enrichment ratios and moderate spatial variability, which indicates that these three elements are greatly influenced by agricultural fertilization and irrigation (Table 1). However, all PTE contents are below the standard limits and, thus, present no risk. In a study by Li [25], the average contents of PTEs in the root soil of the study area were 22.8, 0.225, and 12.2 mg/kg for Pb, Cd, and As, respectively. Thus, the current values represent decreases of 33% for Pb and 90% for Cd compared to those 7 years ago. In a study by Bai [26], the samples exceeding the background values of Pb, Ni, Zn, Cu, Cr, and Cd in Ningxia soil accounted for more than 83% of the total samples, which is higher than the results obtained in this study, and the coefficient of variation for Zn was slightly different.

Except for Cd, none of the other PTE contents in the wolfberries exceeded the standard limits, and only one sample contained Cd exceeding the standard by 0.05 mg/kg. Therefore, the quality of wolfberries in the study area is high, and they can be safely consumed. The test results provide a reference for the safe production of wolfberries based on standard limits for PTE elements. Qi et al. and Geng et al. studied the PTE content in wolfberries from different areas, and only Cd (35.56%) was found

to be present above the standard limit in Qinghai Province[18, 20]. In a study of wolfberry plantations in western China by Xiao et al., it was also concluded that farmland was polluted during years of cultivation, causing, in particular, cadmium pollution, suggesting that wolfberries are subject to excessive Cd exposure, and the mechanism of Cd adsorption by wolfberries should be studied further and considered during planting [27].

For Cd and Cu, the BCF was greater than 1, and their concentrations in the wolfberry fruits are far greater than those in the soil, indicating that absorption and accumulation occur. Petukhov [28] found that the BCF value of Cu in Chinese herbal medicine is generally greater than 1; for example, the BCF for chamomile is 4.67, whereas that for Cd is also higher than 1 (as found in this study). However, Garg et al. [29] determined BCF ranges for Cu and Cd in different crops of 0.011–0.148 and 0.006–0.179, respectively. Possibly, the enrichment of Cu and Cd in Chinese herbal medicines is greater than those in these crops, although this requires further research. Qi et al. [18] found that, compared with those of other PTEs, the enrichment coefficient of Cd in wolfberries was also larger, ranging from 0.318 to 0.903, and the average enrichment coefficients of Ni, As, and Pb were less than 0.1, which is consistent with the results of this study.

In a correlation study of the PTE content of wolfberries and the PTE content and physicochemical soil properties, Qi et al. [18] concluded that, except for Cd in wolfberries and Pb in root soil, there was no clear correlation between PTEs in other wolfberry–soil systems, which is consistent with the results of this study. Wang et al.

[30] found that the adsorption of PTE ions in soil increases with increase in pH, resulting in a decrease in active PTE ions in soil, which affects the absorption of these metals by the wolfberry plants. In this study, this was also observed; however, there was a negative correlation between pH and Cr content, but the correlation was very weak and requires further study. Geng et al. [31] reported that soil organic matter affects the absorption of PTEs (especially As) because it contains a large number of active functional groups, and Chen et al. [12] successfully fitted a linear regression equation for the As content of five crops and that of the root soil. However, good fits were only obtained for corn and red jujube. Possibly, the analysis is limited to these crop species or the study involved too few sampling points. Adams et al. [32] reported that the Cd content and soil pH are the main factors affecting the Cd content in wheat and barley using multiple regression analysis. At the same time, McBride [33] obtained an equation by fitting that showed that the soil Cd content and pH significantly affected the Cd content of lettuce, beet, and maize leaves. Zhu et al. [34] also obtained a regression equation for the Cd content of Sanchi roots as a dependent variable and Zn concentration and pH value of the soil as independent variables, achieving $r = 0.765$ at $p < 0.01$. However, although many previous studies have proven the applicability and universality of this method, the multivariate linear relationship between Cd content of wolfberries and the soil PTE content and physicochemical properties was not strong, although those of other metals were. This may be a result of the limited sample size. However, if this method were used for the analysis of widely planted crops, more samples could be obtained, and the results could be improved. In addition, the determination of more soil physicochemical

properties and an increase in the number and relevant types of independent variables could increase model accuracy.

In this study, the dispersion of As in the soil was found to be significant, whereas Chen et al. [12] found that the As content in soil in Xinjiang and other places in China showed significant spatial autocorrelation. Therefore, we cannot exclude a spatial autocorrelation in the As content in soil. Possibly, this was not observed in this study because of the small sample size or inappropriate sample point selection. The spatial variability of soil As content was assessed to be moderately correlated, which may be caused by the superposition of structural factors (such as topography, soil type, parent material, climate) and random factors (such as fertilization, cultivation, planting system, land use intensity, and other human activities), which is similar to the trend obtained by Moran's I analysis. The nugget of each PTE indicates that there are positive basal effects caused by sampling error, short-distance variation, and random variations in the soil of the study area [35]. The research area used by Bai et al. [26] overlaps with our research area. Because of the high density of research points, the overall trend of overlapping regions is the same, but different results were obtained, which is mainly manifested in the hierarchy and variability of the interpolation map. For example, compared with our Ni distribution map, that of Bai et al. has four content levels, whereas, in the same area, our map only contains two content levels. Considering that the analysis of more common crops would enable the analysis of more root soil, this hierarchy gap could be avoided. Geng [20] evaluated the PTE content of the soil in a wolfberry plantation in Qinghai. Using the potential ecological risk assessment method, 38.9% of the sampling

sites were assessed to be medium risk for Ni, whereas most of the other PTEs were rated as low risk. A high Hg content in the soil may be a major feature of wolfberry plantations. To date, studies have not investigated the potential ecological risks of Hg in the soil in this study area, so the Hg risk grade presented here will enable the development of risk management strategies at the government level. In this study, we innovatively combined the risk model with Kriging interpolation to visualize the risks, thus providing a reference to monitor changes in soil PTE content and improvements in soil health.

The Chinese government plans to increase the area used for cultivating wolfberries in the Ningxia Hui Autonomous Region, making the need to forecast and analyze the PTE content and ecological risk of wolfberries in the study area crucial. Because the planting of wolfberries is not spatially continuous, which is not consistent with the requirements for data in geostatistical spatial interpolation, but the soil indicators are continuous, we attempted to use the predicted PTE contents of wolfberries after linear fitting of the soil data for interpolation of the study area. Although the results contained errors, this novel concept for the interpolation of PTE concentrations and the health risk of crops is promising. In previous studies, the health risks of tomatoes and Chinese rice were assessed, and this method can also be combined with geospatial analysis to visualize the health risk presented by different crop cultivation areas [36-37]. The resulting interpolation map can provide a reference for the site selection of wolfberry cultivation sites, as well as legislation for PTE standards for wolfberries.

4 Materials and Methods

4.1 PTE determination

The Ningxia Hui Autonomous Region is the main production area of Chinese wolfberries and the origin of this plant; specifically, Zhongwei is a key planting area. Shapotou District and Zhongning County in Zhongwei are located from 104°17’ E to 106°7’ E and 36°6’ N to 37°50’ N [38]. As a result of its suitable latitude, long sunshine period, large diurnal temperature range, and abundant water resources, this region has been developed into a high-quality planting area [30-40]. Therefore, these two areas were used in this study (Fig. 5). Using the spot placement method [41], 37 wolfberry samples (Fig. 5) and surface soil (from the surface to 20-cm depth, approximately 300 g) of the soil around the wolfberry root system was collected.

The instrumentation used for PTE analysis is listed in Supplementary Table S8 online, and the methods of determination, basis, units, and detection limits for PTEs, as well as the pH, organic matter content, and cation exchange capacity of the soil, are listed in Supplementary Table S9 online. The collected soil samples were spread flat to allow the removal of foreign objects such as stones and animal and plant residues in the soil samples. The samples were allowed to dry in the air and were not exposed to direct sunlight. Then, they were crushed with wooden sticks, any impurities were removed, mixed, and crushed. The samples were selected using the quartering method. Each sample was passed through a 10-mesh (2 mm) nylon sieve, and all the sieved samples were placed on a colorless polyethylene film, fully stirred and mixed; then, two parts were selected following the quartering method. One part was transferred to the sample

inventory, and the other part was finely ground. The finely ground sample was then divided into two parts by the quartering method, and the sample was further ground and passed through a 100-mesh (0.149 mm) sieve. These samples were used for analysis.

Each wolfberry weighed about 0.2 g averagely, and each sample was accurately weighed into a digestion tube. Then, 10 mL of mixed acid (HNO_3:$HClO_4$ = 4:1) was placed in a 50-mL digestion tube, stoppered, sealed, and left overnight [42]. For each sample, a parallel experiment was carried out, and standard addition and reagent blank samples were prepared. The next day, the plug was removed, and 4 mL of 30% H_2O_2 was added to each digestion tube. The tube was placed on a plate in a graphite furnace to catch the acid and heated. The graphite furnace was programmed to increase from room temperature to 60 °C, from 60 to 120 °C, and, then, to 180 °C. Subsequently, the sample was held at this temperature for 4–6 h. After the acid had been completely removed, the digestion tube was cooled to room temperature, and the sample plug was added. Before the metal determination, ultrapure water was added to the digestion tube several times in small amounts, and the tube was shaken to dissolve the deposited crystals, transferred to a 10-mL sample tube, and, again, shaken well.

4.2 Bioconcentration factor of wolfberries

To compare the ability of different PTEs to migrate from the soil into the wolfberries, the bioconcentration factor (BCF) was used [29]. The BCF was calculated using equation (1). If BCF ≤ 1.00, a plant absorbs but does not accumulate metals. However, if BCF > 1.00, a plant accumulates metals [28]. Thus, this is an indicator that characterizes the degree of concentration or enrichment of a chemical substance by an

organism.

$$BCF = \frac{C_i}{C_{soil}} \quad (1)$$

Here, C_i is the concentration of different PTEs in wolfberry fruit (mg/kg), and C_{soil} is the concentration of PTEs in the soil (mg/kg).

4.3 Multiple linear regression

Multiple linear regression was used to analyze the linear relationship between different dependent and multiple independent variables. F-tests were used to assess model quality based on the selected independent variables; because the number of samples was small, the α value was set to 0.10–0.15 [43]. In this study, the PTE contents of the wolfberries were used as dependent variables, and the PTEs in the soil around the root and related physical and chemical properties (pH, organic matter, and cation exchange capacity) were introduced as independent variables. A stepwise regression method was used to perform multiple linear regression. The general form of the equation is given by equation (2).

$$Y = b_1X_1 + b_2X_2 + b_3X_3 + \cdots + b_xX_n \quad (2)$$

Here, Y is the predicted dependent variable (PTE content in wolfberry samples), b_0 to b_x are partial regression coefficients, and X_1 to X_n are different independent variables (for example, soil PTE content and other physical and chemical properties).

4.4 Normality tests and conversion

As in statistics, in geostatistics, we assume that a sample obeys the normal distribution [35]. The normality tests revealed that, of those of the eight PTEs studied, the concentration distributions of Ni, Zn, and As in the soil were normal, and the *p*-

values of the other five PTEs were all less than 0.05. In ArcGIS 10.0, three methods are provided for the normal transformation of the original data: log, Box–Cox, and Arcsin. As shown in Supplementary Table S10 onlie, after logarithmic conversion, the concentrations of Cu and Cr in the soil were normally distributed. In contrast, the Pb and Hg concentration data in the soil were imported into Minitab, and Box–Cox transforms to fit to the optimal normal distribution was carried out. In the Box–Cox plot, the λ factor of the Pb concentration in the soil was λ = -0.66 in the λ curve (Supplementary Fig. S2 and Fig. S3 online) and that for the Hg concentration in the soil was λ = 0.41, yielding a normally distribution. The *p*-value of the Cd concentration in the soil after conversion was also less than 0.05.

4.5 Spatial autocorrelation analysis

In this study, ArcGIS (version 10.0) was used to analyze the spatial autocorrelation of the concentration of seven detected PTEs in the soil. Spatial autocorrelation refers to the potential interdependence between the observed data of certain variables in the same partition. Moran's I, a global aggregation characteristic, is the most common statistic used to characterize spatial autocorrelation analysis. After the variance has been normalized, the composite index lies between -1 and 1. When Moran's I > 0, there is a positive spatial correlation (clustering), and larger I values indicate a stronger spatial autocorrelation; when Moran's I < 0, there is a negative spatial correlation (dispersion), and smaller indices indicate greater spatial differences. When Moran's I = 0, the space is distributed randomly [44].

4.6 Semivariogram model

Geostatistics is based on the theory of regionalized variables, for which a function of the variation (a semivariogram) is the basic tool. This can be used to describe the structural characteristics and randomness of the key elements of the soil or the method of spatial correlation and dependence [12]. The general form of a semivariogram is given by equation (3).

$$\gamma^*_{(h)} = \frac{1}{2N(h)} \sum_{i=1}^{N(h)} [Z(x_i) - Z(x_i + h)]^2 \quad (3)$$

Here, h is the spatial separation of two sample points, $Z(x_i)$ is the observed value for soil sample $Z(x)$ at spatial position x_i, $Z(x_i + h)$ is another observed value for a soil sample $Z(x)$ separated from the original data point by distance h, $\gamma^*_{(h)}$ is the experimental function of variation of the observations separated by distance h; that is, the degree of dissimilarity between points $Z(x_i)$ and $Z(x_i + h)$, and $N(h)$ is the number of sampling point pairs. GS+ 10 (Gammadesign Software) was used to process the seven normal or normally transformed PTE concentrations, select the theoretical model, such as Gaussian or spherical model, for the semivariogram, and calculate the parameters for the determined model. These data were used for the Kriging interpolation and spatial distribution modeling in GS+ 10 and ArcGIS 10.0.

4.7 Soil potential ecological risk index method

To evaluate the PTE pollution in soil, we used the potential ecological risk index proposed by Hakanson [45]. This method is uses principles of sedimentology, PTE behavior, and environmental behavior to evaluate the pollution of soil or sediments by PTEs [46]. In addition to the PTE content of the soil, the risk index also considers factors, such as multi-element synergy, toxicity, pollutant concentration, and environmental

sensitivity to PTE pollution, and adopts a comparable and equivalent attribute index classification method for evaluation [47]. The potential ecological risk index is calculated using equations (4) and (5).

$$E_{\text{total}} = \sum E_i \tag{4}$$

$$E_i = T_i \times \frac{C_i}{C_{i-ref}} \tag{5}$$

Here, E_{total} is the potential ecological risk index, E_i is the individual coefficient of potential ecological risk of metal element i, T_i is the toxicity response coefficient of the metal element (Supplementary Table S11 online), C_i is the actual measurement of the metal element i in the surface soil concentration (mg/kg), C_{i-ref} is the reference value, and the background value is usually used (Supplementary Table S11 online) [19].

Data Availability

All data generated or analyzed during this study are included in this published article.

References

[1] Pettry D. E. et al. Soil pollution and environmental health. Health Services Reports, 88(4), 323-327 (1973).

[2] Mohammed M.S., A. A. M. Sallam, & Aleid, S. M. Assessment of soil PTE hazards of cultivated soil irrigated with different irrigation water qualities in Al-Hassa Oasis, Kingdom of Saudi Arabia. World Rural Observations, 6(4), 12-22 (2014).

[3] Liu Yang et al. PTE accumulation in crops and its relationships with nitrogen and phosphorus in different-age reclaimed farmlands in tidal flat area. Asian Journal

of Ecotoxicology, 13(6), 186-201. DOI: 10. 7524 /AJE. 1673 − 5897. 20171221001 (2018).

[4] Ander, E. L., Johnson, C. C., Cave, M. R., Palumbo-Roe, B., Nathanail, C. P., & Lark, R. M. Methodology for the determination of normal background concentrations of contaminants in English soil. Science of the Total Environment, 454-55, 604-618 (2013).

[5] Petrik, A., Thiombane, M., Albanese, S., Lima, A., & De Vivo, B. Source patterns of Zn, Pb, Cr and Ni potentially toxic elements (PTEs) through a compositional discrimination analysis: A case study on the Campanian topsoil data. Geoderma, 331, 87-99 (2018).

[6] Ungureanu, T., Iancu, G. O., Pintilei, M., & Chicoș, M. M. Spatial distribution and geochemistry of PTEs in soils: A case study from the NE area of Vaslui county, Romania. Journal of Geochemical Exploration, 176, 20-32 (2016).

[7] Vasu, D., Singh, S.K., & Sahu, N. Assessment of spatial variability of soil properties using geospatial techniques for farm level nutrient management. Soil and Tillage Research, 169, 25–34 (2017).

[8] Zou, J., Dai, W., Gong, S., & Ma, Z. Analysis of spatial variations and sources of PTEs in farmland soils of Beijing suburbs. PLoS One, 10(2), e0118082 (2015).

[9] Miransari, M. T., Ghare Maleki, H., Besahrati, M. H., & Rasuli Sadaghiani, A. T. Using pseudomonas spp. and arbuscular mycorrhizal fungi to alleviate the stress of zinc pollution by corn (zea may L.) plant. Journal of Plant Nutrition, 36(13), 2061-2069. DOI: 10.1080/01904167.2013.816733 (2013).

[10] Zhan Chen, Xiao-ke Wang, Zhang-zhong Feng, Qin Xiao, & Xiao-nan Duan. Impact of elevated O3 on soil microbial community function under wheat crop. Water, Air, &Soil Pollution, 198(1-4), 189-198 (2009).

[11] Behnam Keshavarzi, Farid Moore, Maryam Ansari, Meisam Rastegari Mehr, Helena Kaabi, & Maryam Kermani. Macronutrients and trace metals in soil and food crops of Isfahan Province, Iran. Environ Monit Assess. 187(4113), 1-22. DOI: 10.1007/s10661-014-4113-y (2015).

[12] Yun-fei Chen et al. Spatial distribution of soil arsenic and arsenic enrichment in crops in the Oasis region of the southeastern Tarim Basin. Environmental Science, 41(1), 438-448 (2020).

[13] Ming Yang, Kwok-Fai So, Amy Cheuk Yin Lo, & Wai Ching Lam. The effect of Lycium barbarum polysaccharides on pyroptosis-associated amyloid β1-40 oligomers-induced adult retinal pigment epithelium 19 cell damage. International Journal of Molecular Sciences, 21(4658), 1-16. DOI: 10.3390/ijms21134658 (2020).

[14] Lia Mara Grosso Neves et al. Lycium barbarum polysaccharide fraction associated with photobiomodulation protects from epithelium thickness and collagen fragmentation in a model of cutaneous photodamage. Lasers in Medical Science. DOI: 10.1007/s10103-020-03132-w (2020).

[15] Cui-cui Shao, Yuan-xi Deng, & Bei-bei Yang. The nutritional value and health function of Lycium barbarum and its application progress. Journal of Anhui Agricultural Science, 26(17), 39-41. DOI: 10.16377/j.cnki.issn1007-

7731.2020.10.0 (2020).

[16] Na Li. The research on extraction technology of pigment, total flavonoids and total polysaccharides in Lycium Chinese. Henan University of Technoligh (2006).

[17] Qi-zhi Peng. Determination of five metal elements in Meldar and assessment on its health risk. China Medicine and Pharmacy, 4(9),121-123 (2014).

[18] Guo-liang Qi et al. Comparative study on heavy mental elements in soil and fruit of Lycium bararum L. in different regions. Northern Horiculture, 15, 161-164 (2014).

[19] China National Environmental Monitoring Centre. Background values of soil elements in China. China Environmental Science Press, Beijing (1990).

[20] Gui-Gong, Geng. Study on PTE content and soil association of Lycium barbarum in Qinghai province. Agriculture and Animal Husbandry College, University of Qinghai (2018).

[21] Wilding, L. P. Spatial variability: its documentation, accommodation, and implication to soil survey. In: Nielsen D R, Bouma J. Wageningen: Pudoc, 166-194 (1985).

[22] Chinese Pharmacopoeia Commission. Chinese Pharmacopoeia. The Medicine Science and Technology Press of China, Beijing (2015).

[23] Ministry of Foreign Trade and Economic Cooperation. Green standards of medicinal plants and preparations for foreign trade and economy (WM/T2—2004). China Standards Press, Beijing (,2005).

[24] Jian-rong Kai et al. A comparative study of 49 inorganic elements in red, black and

yellow Lycium barbarum. Food and Fermentation Industries, 46(9), 152-157. DOI: 10.13995/j.cnki.11-1802/ts.02331 (2020).

[25] Yun-xiang Li, Ying Ke, Jian-hang Luo, Xiao-qun Chen, Xue-jun Zhang. Evaluation and present situation of soil environmental quality in the major Wolfberry production areas of Ningxia. Soil and Fertilizer Sciences in China, 2, 21-26. DOI: 10. 11838/sfsc. 20160204 (2016).

[26] Yi-ru Bai, Xing Zhang, Yun-peng Zhao, & You-qi Wang. Spatial distribution characteristics and source apportionment of soil PTEs in Chinese Wolfberry land Based on GIS and the Receptor Model. Environmental Science, 40(6), 2885-2894. DOI: 10. 13227 /j. hjkx. 201811047 (2019).

[27] Ming Xiao et al. Cadmium accumulation in soil and risk prediction in the Qaidam Basin. Journal of Plant Nutrition and Fertilizer, 20(5), 1271-1279. DOI: 10. 11674/zwyf.2014.0524 (2014).

[28] Petukhov, A. S., Kremleva, T. A., Petukhova, G. A., & Khritokhin, N. A. Translocation of PTEs in Herbs under Urban Anthropogenic Pollution Conditions. Environmental Processes, 7(4), 11731196. DOI: 10.1007/s40710-020-00470-3 (2020).

[29] Garg, V. K. et al. PTEs bioconcentration from soil to vegetables and assessment of health risk caused by their ingestion. Biological Trace Element Research, 157(5), 256-265. DOI: 10.1007/s12011-014-9892-z (2014).

[30] Yan-xia Wang, Jun Zhao, & Guo-hu Zhao. Analysis and evaluation of PTE content of vegetable garden soil in Anning District of Lanzhou city. Journal of Anhui

Agricultural Science, 35(19), 5804-5805 (2007).

[31] An-jing Geng et al. Research progress on the factors affecting the migration of Arsenic in soil and crop system. Quality and Safety of Agricultural Products, 3, 24-30 (2020).

[32] Adams, M. L., Zhao, F. J., McGrath, S. P., Nicholson, F. A., & Chambers, B. J. Predicting cadmium concentrations in wheat and barley grain using soil properties. Journal of Environmental Quality, 33(2), 532–541 (2004).

[33] McBride, M. B. Cadmium uptake by crops estimated from soil total Cd and pH. Soil Science, 167(1), 62–67. DOI: 10.1097/00010694-200201000-00006 (2002).

[34] Mei-lin Zhu et al. Cadmium accumulation in Panax notoginseng: levels, affecting factors and the non-carcinogenic health risk. Environ Geochem Health, 38, 423-435 (2016).

[35] Xin-qi, Zheng, Li-na, Lv. Geostatistics (Spatial Statistical Analysis). Science Press, Beijing, pp. 21-23 (2018).

[36] Hong-wen Dai, Xiu-xian Song, Bai-fei Huang, & Jun-liang Xin. Health risks of PTEs to the general public in Hengyang, China via consumption of rice. Human and Ecological Risk Assessment: An International Journal, 43(8), 1-33. DOI: 10.1080/10807039.2016.1207156 (2016).

[37] E. Işıl Arslan Topal, Murat Topal, Erdal Öbek. Assessment of PTE accumulations and health risk potentials in tomatoes grown in the discharge area of a municipal wastewater treatment plant. International Journal of Environmental Health Research, 1369-1619. DOI: 10.1080/09603123.2020.1762071 (2020).

[38] Fen-fen Yue. Problems and countermeasures of apple and Wolfberry industry development in Shapotou District of Zhongwei city. Ningxia Agriculture and Forestry Science and Technology, 60(6), 30-31. DOI: 10.3969/j.issn.1002-204x.2019.06.010 (2019).

[39] Hua-li Huo, Pu-xing Liu, & Ke-xin Zhang. Spatio-Temporal change of sunshine hour in Ningxia during the past 50 years. Journal of Desert Research, 31(2), 521-524 (2011).

[40] Zhang-li Dang, Li-jing Wang, & Wan-zhong Mao. Analysis on Meteorological conditions of Lycium barbarum planting in Zhongwei City. Shaanxi Journal of Agricultural Sciences, 65(12), 86-89 (2019).

[41] Guan-jiu Hu, Su-lan Chen, & Juan Huang. Discussions on sampling sites for regional soil pollution investigation. Journal of Geology, 36(2), 165-169. DOI: 10. 3969 /j. issn. 1674-3636. 2012. 02. 165 (2012).

[42] Liang Fu, Shu-Yun Shi, & Xiao-Qing Chen. Accurate quantification of toxic elements in medicine food homologous plants using ICP-MS/MS. J. Food Chemistry, 245, 692-697. DOI: org/10.1016/j.foodchem.2017.10.136 (2018).

[43] Zhen-qiu, Sun, Yong-yong, Xu. Medical Statistics, fourth ed. People's Medical Publishing House, Beijing, pp. 236 (2014).

[44] Ai-li, Liu, Pei-fa, Wang, & Yuan-yuan, Ding. Introduction to Geostatistics. Science Press, Beijing, pp. 50-95 (2012).

[45] Hakanson, L. An ecological risk index foe aquatic pollution control-A sedimentological approach. Water Res, 14(8), 975-1001 (1980).

[46] Sunitee Gohain Baruah et al. Heavy mental(loid)s contamination and health risk assessment of soil-rice system in rural and peri-urban areas of low brahmaoutra valley, northeast India. Chemosphere, 266, 1-10. DOI: 10.1016/j.chemosphere.2021.129150 (2021).

[47] Ali Keshavarzi, Vinod Kumar. Spatial distribution and potential ecological risk assessment of PTEs in agricultural soils of Northeastern Iran. Geology, Ecology, and Landscapes, 4(2), 87-103. DOI: 10.1080/24749508.2019.158758 (2020).

Acknowledgments

The present study was financially supported by the National Natural Science Foundation of China (grant nos. 21966025 and 21667023), the Ningxia Key Research and Development Program (grant nos. 2019BFG02020) and the Ministry of Education 'ChunHui' plan project (grant nos. Z2016068).

Authors' Contributions

TZ, YZ and MZ conceived and designed the experiments. YZ and MZ performed the experiments. JQ and YW analyzed the data. JQ and JY provided the analysis tools. CM provided the ArcGIS Desktop 10 software. TZ wrote the manuscript. All authors read and approved the final manuscript.

Competing Interests

The authors declare no competing interests.

Tables and Figures

Table 1 Descriptive statistics of soil PTEs contents in research area

	Ni	Cu	Zn	As	Cd	Pb	Cr	Hg

Detection rate (%)	100	100	100	100	94.6	100	100	100
Mean ± SD ($mg \cdot kg^{-1}$)	40.95± 9.42	5.27± 1.61	42.46± 6.21	8.36± 1.59	0.026± 0.024	23.00± 9.00	52.89±2 0.469	0.069± 0.036
Min ($mg \cdot kg^{-1}$)	21	3	30	4.73	0	14	28	0.0108
Max ($mg \cdot kg^{-1}$)	60	10	55	11.2	0.13	53	114	0.241
Coefficient of Variation (%)	23	30.55	14.63	19.06	92.72	39.12	38.7	51.96
[a] Background value ($mg \cdot kg^{-1}$)	38.4	22.1	58.8	11.9	0.112	20.6	60	0.02
[a] Limited standard value ($mg \cdot kg^{-1}$)	190	200	300	20	0.8	240	350	1
[b] The enrichment proportion	1.07	0.24	0.72	0.7	0.23	1.12	0.88	3.47
[c] The enrichment ratio	64.86	0	0	0	2.7	51.35	35.14	97.3

[a] From *Background values of soil elements in China*.

[b] The enrichment ratio is the ratio of the sample number over the background value to the total sample number.

[c] The enrichment proportion=average/background value.

Table 2 Descriptive statistics of wolfberry PTEs contents in research area

	Ni	Cu	Zn	As	Cd	Pb	Cr	Hg

Mean ± SD (mg·kg^{-1})	0.88±0.44	8.70±2.70	19.56±6.41	0.20±0.23	0.10±0.07	0.35±0.27	2.62±1.20	[a]u
Max (mg·kg^{-1})	2.52	14.49	35.35	0.81	0.35	0.96	5.32	[a]u
Min (mg·kg^{-1})	0.21	2.29	10.98	0	0.03	0	0.17	[a]u
Detection rate (%)	100	100	100	59.46	100	91.89	100	[a]u
Standard exceeding ratios (%)	[b]-	0	[b]-	0	2.7	0	[b]-	[a]u

[a] u indicates that it is not detected.

[b] - indicates that the limit standard is not specified in China.

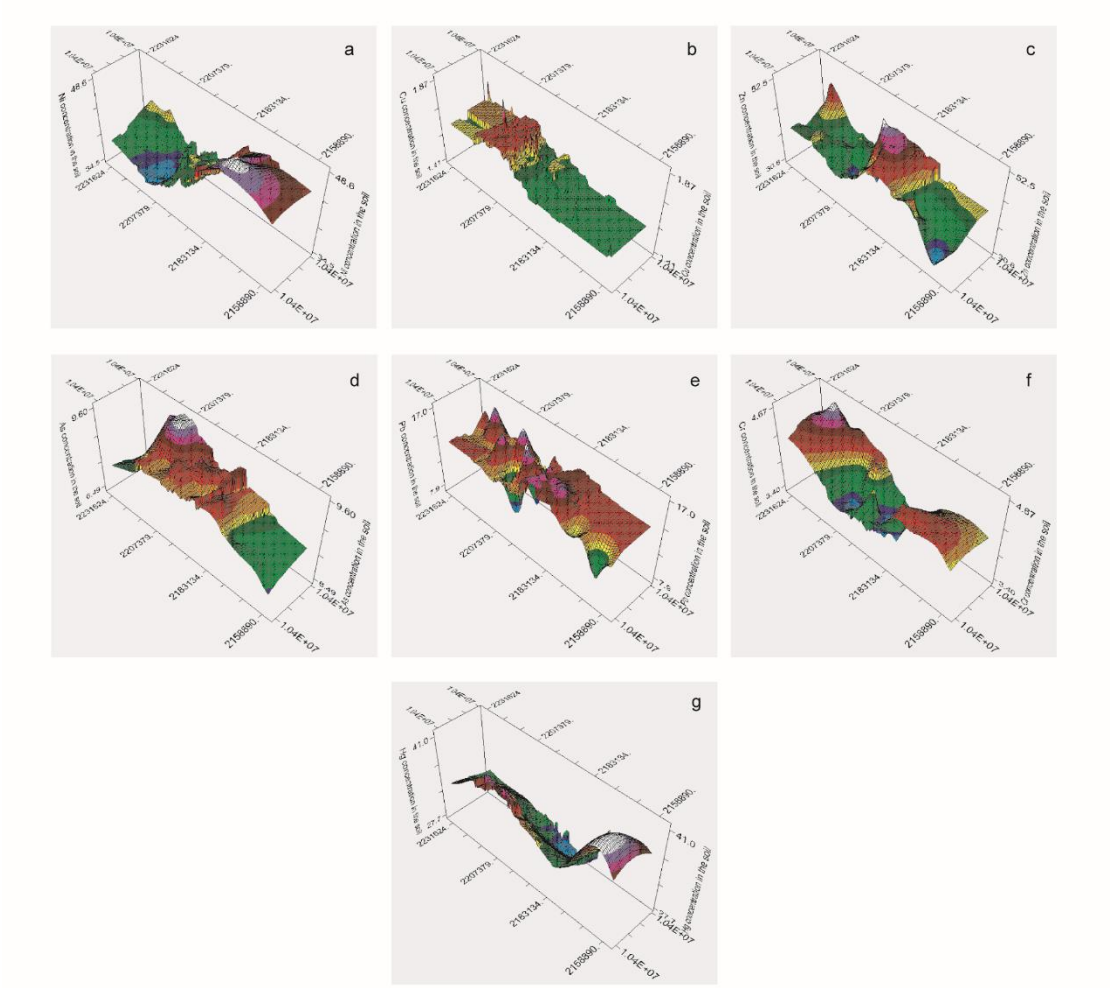

Figure 1 3D ordinary Kriging prediction chart of soil PTEs content in the sampling area (GS+ 10.0)

Note: This Figure shows the content of PTEs in the soil of the distribution area. The higher the height is, the higher the content is. Each graph represents different PTEs, a: Ni, b: Cu, c: Zn, d: As, e: Pb, f: Cr, g: Hg. In the east–west direction, the seven types of PTEs show undulating distribution patterns within the studied range, and only one peak appears the interpolation diagrams of As and Cu, whose concentrations are high in the central region and low in the east and west regions. The distribution diagram for Pb is more volatile than those of the other PTEs, showing more peaks in the east and gentle peaks in the west. In the northwest direction, there is no clear trend for Cu nor Cr, whereas the trends for Ni, Zn, Pb, and As are high in the north and low in the south. In contrast, uniquely, Hg has a high distribution in the south and low distribution in the north. The highest value for

Ni appeared in the west wave crest, and the lowest value was located in the trough in the southeast. The Cu peak appears on the east side of the wave crest, whereas the lowest point is located in the west surrounded by other low values. The peak and valley values for Zn both appear in the middle region, the distance between the extreme points is close, and the Zn content changes significantly. The highest value for As appeared in the northeast, and the lowest value appeared in the west. The strong fluctuation in Pb content, whose distribution shows multiple peaks. Concerning the Cr distribution, there is a peak in the east region, a low value in the middle region, and a small peak in the middle low-content region. The Hg content did not show any sudden increases or decreases, but a peak appeared in the western region, and the lowest point appeared north of the central region.

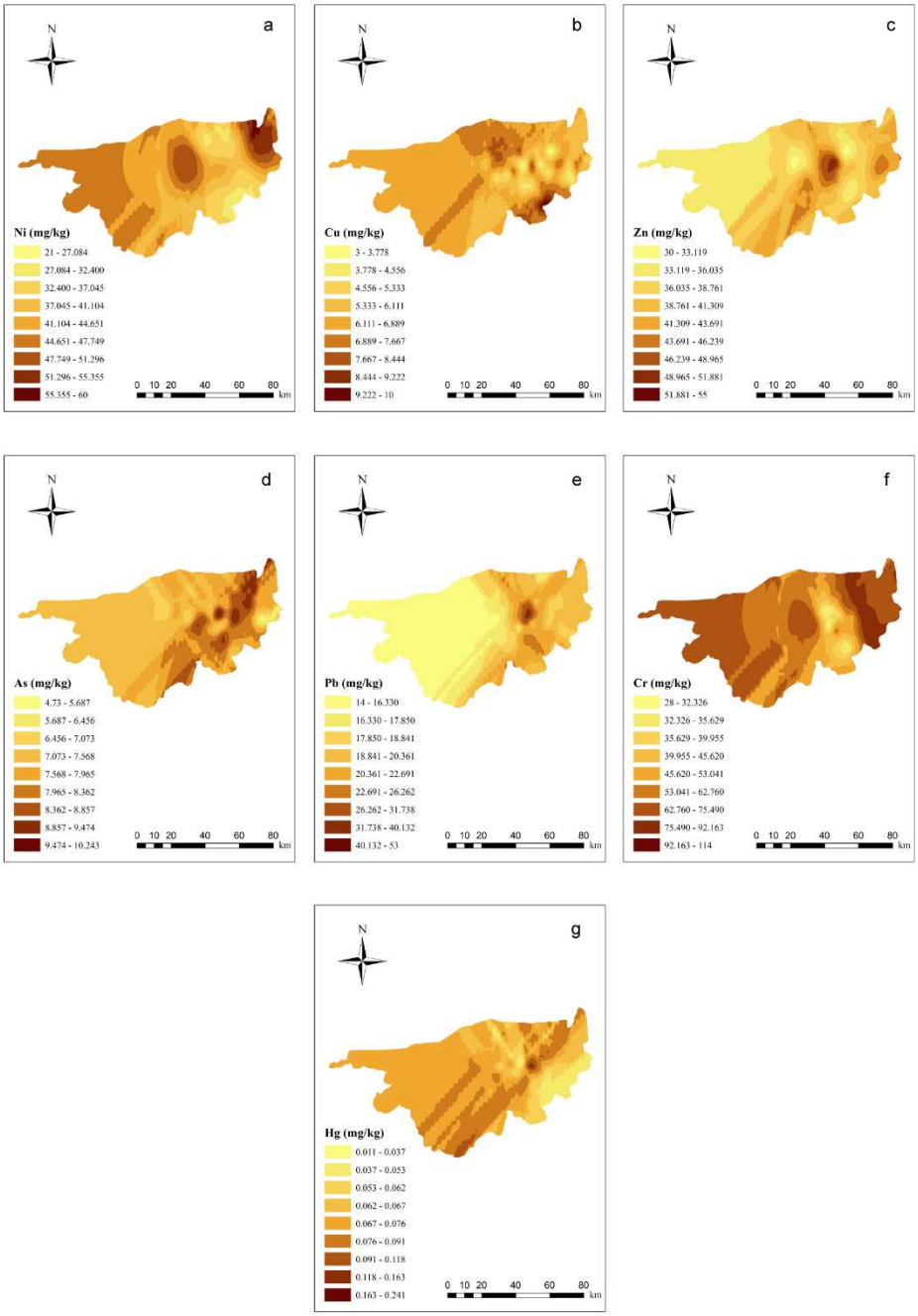

Figure 2 Ordinary Kriging prediction chart of soil PTEs content in the study area (ArcGIS 10.0)

Note: This Figure shows the content of PTEs in the soil of the study area. Different colors represent different contents. Each graph represents different PTEs, a: Ni, b: Cu, c: Zn, d: As, e: Pb, f: Cr, g: Hg. ArcGIS Desktop 10 software with the authorization number of EFL564098460.

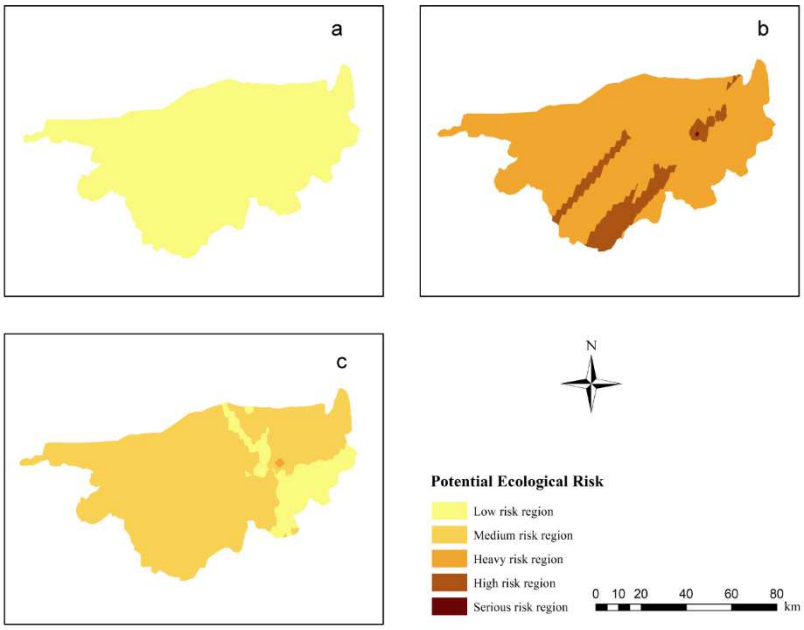

Figure 3 Ordinary Kriging prediction chart of potential ecological risk of soil PTEs in the study area (ArcGIS 10.0)

Note: (a) is the prediction chart of potential ecological risk of As Cr Cu Ni Zn and Pd, (b) is the prediction chart of potential ecological risk of Hg, and (c) is the prediction chart of potential ecological total risk. ArcGIS Desktop 10 software with the authorization number of EFL564098460.

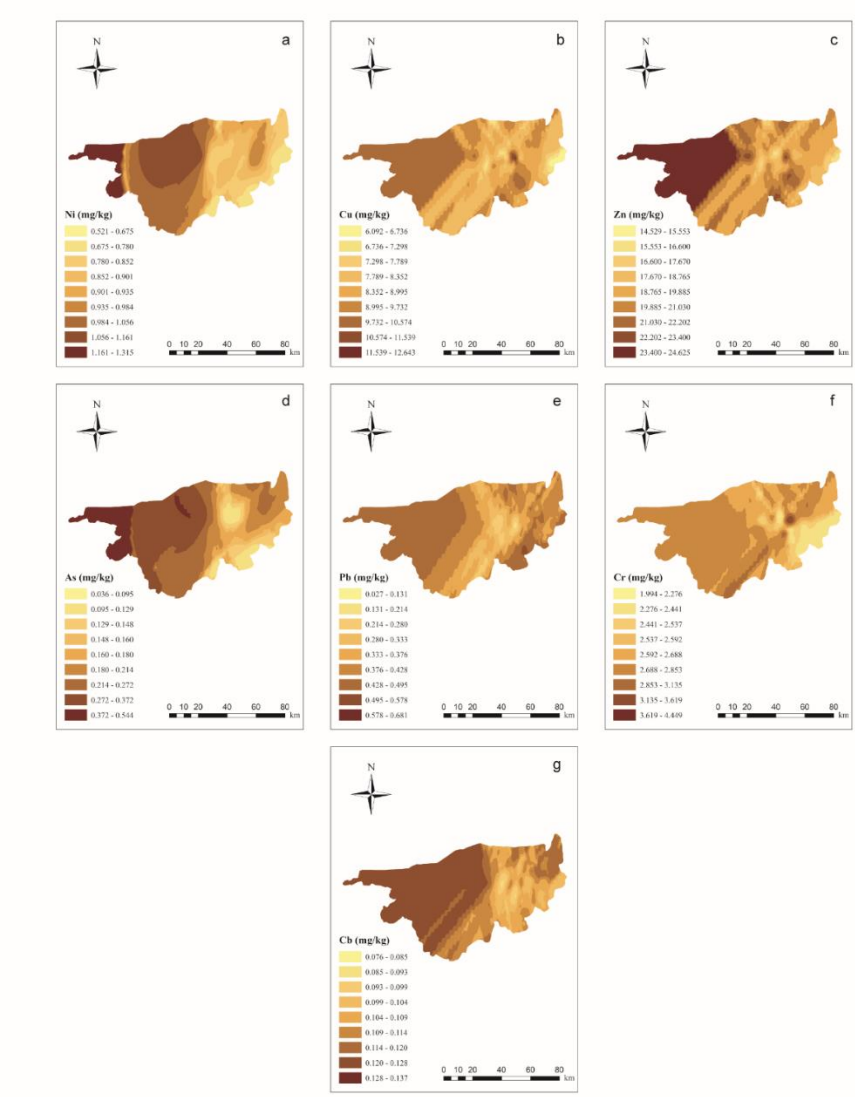

Figure 4 Ordinary Kriging prediction chart of wolfberry PTEs content in the study area (ArcGIS 10.0)

Note: This Figure shows the content of PTEs (based on the soil) in the wolfberry of the study area. Different colors represent different contents. Each graph represents different PTEs, a: Ni, b: Cu, c: Zn, d: As, e: Pb, f: Cr, g: Cd. ArcGIS Desktop 10 software with the authorization number of EFL564098460.

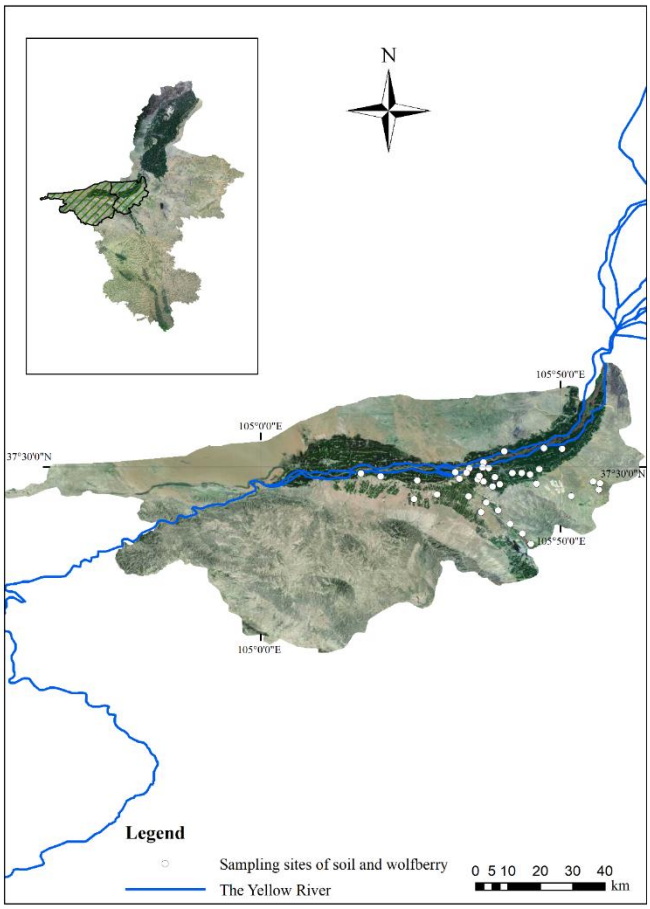

Figure 5 Geomorphology of the study area and sampling sites distribution

Note: The southern part of the study area is mountainous area, the northwest part is desert area, and the dark green area along the Yellow River in the middle part is plain cultivated area. ArcGIS Desktop 10 software with the authorization number of EFL564098460

Figures

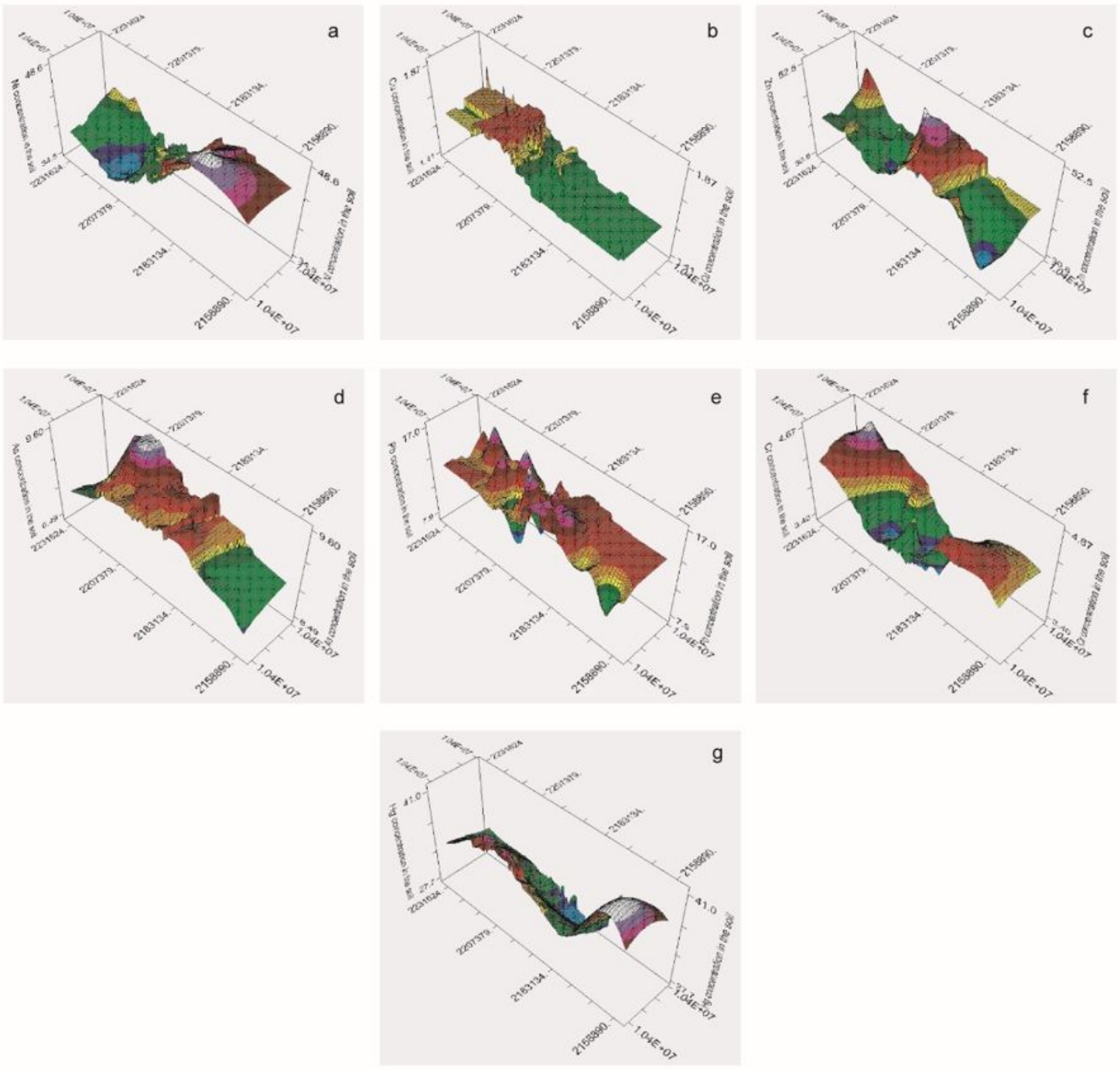

Figure 1

3D ordinary Kriging prediction chart of soil PTEs content in the sampling area (GS+ 10.0) Note: This Figure shows the content of PTEs in the soil of the distribution area. The higher the height is, the higher the content is. Each graph represents different PTEs, a: Ni, b: Cu, c: Zn, d: As, e: Pb, f: Cr, g: Hg. In the east–west direction, the seven types of PTEs show undulating distribution patterns within the studied range, and only one peak appears the interpolation diagrams of As and Cu, whose concentrations are high in the central region and low in the east and west regions. The distribution diagram for Pb is more

volatile than those of the other PTEs, showing more peaks in the east and gentle peaks in the west. In the northwest direction, there is no clear trend for Cu nor Cr, whereas the trends for Ni, Zn, Pb, and As are high in the north and low in the south. In contrast, uniquely, Hg has a high distribution in the south and low distribution in the north. The highest value for Ni appeared in the west wave crest, and the lowest value was located in the trough in the southeast. The Cu peak appears on the east side of the wave crest, whereas the lowest point is located in the west surrounded by other low values. The peak and valley values for Zn both appear in the middle region, the distance between the extreme points is close, and the Zn content changes significantly. The highest value for As appeared in the northeast, and the lowest value appeared in the west. The strong fluctuation in Pb content, whose distribution shows multiple peaks. Concerning the Cr distribution, there is a peak in the east region, a low value in the middle region, and a small peak in the middle low-content region. The Hg content did not show any sudden increases or decreases, but a peak appeared in the western region, and the lowest point appeared north of the central region.

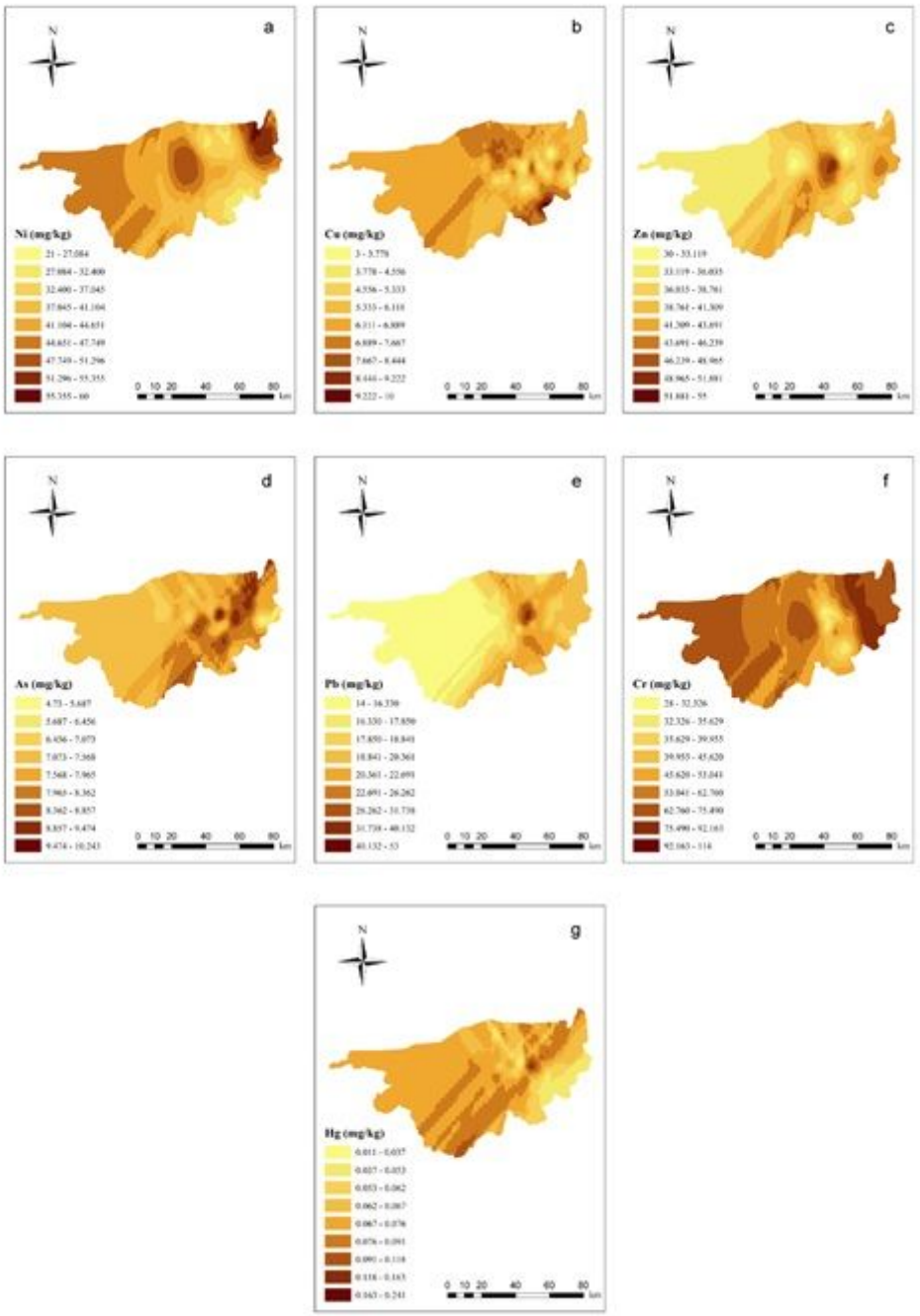

Figure 2

Ordinary Kriging prediction chart of soil PTEs content in the study area (ArcGIS 10.0) Note: This Figure shows the content of PTEs in the soil of the study area. Different colors represent different contents. Each graph represents different PTEs, a: Ni, b: Cu, c: Zn, d: As, e: Pb, f: Cr, g: Hg. ArcGIS Desktop 10 software with the authorization number of EFL564098460. Note: The designations employed and the presentation of the material on this map do not imply the expression of any opinion whatsoever on the part of Research Square concerning the legal status of any country, territory, city or area or of its authorities, or concerning the delimitation of its frontiers or boundaries. This map has been provided by the authors.

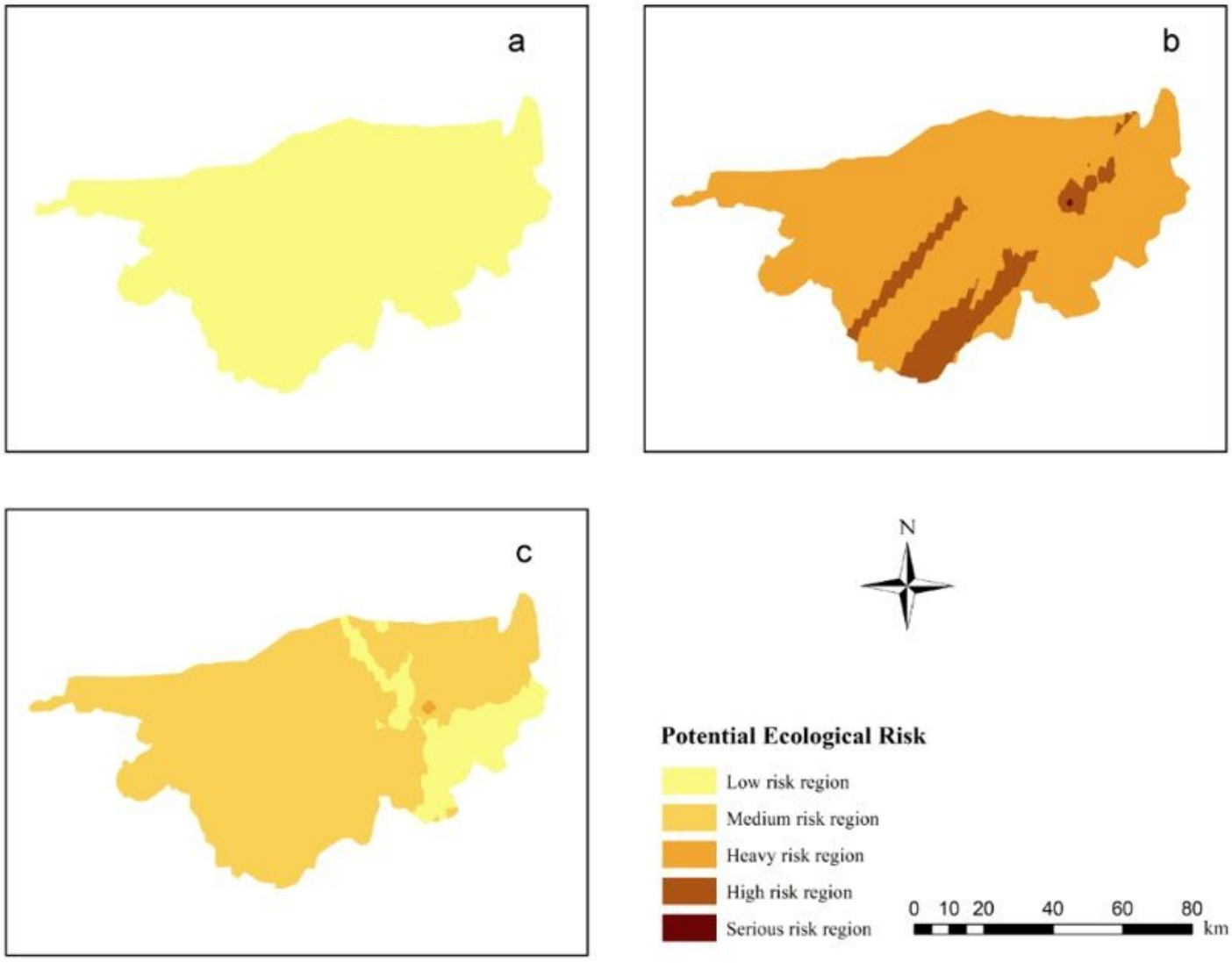

Figure 3

Ordinary Kriging prediction chart of potential ecological risk of soil PTEs in the study area (ArcGIS 10.0) Note: (a) is the prediction chart of potential ecological risk of As Cr Cu Ni Zn and Pd, (b) is the prediction chart of potential ecological risk of Hg, and (c) is the prediction chart of potential ecological total risk. ArcGIS Desktop 10 software with the authorization number of EFL564098460. Note: The designations employed and the presentation of the material on this map do not imply the expression of any opinion whatsoever on the part of Research Square concerning the legal status of any country, territory, city or area or of its authorities, or concerning the delimitation of its frontiers or boundaries. This map has been provided by the authors.

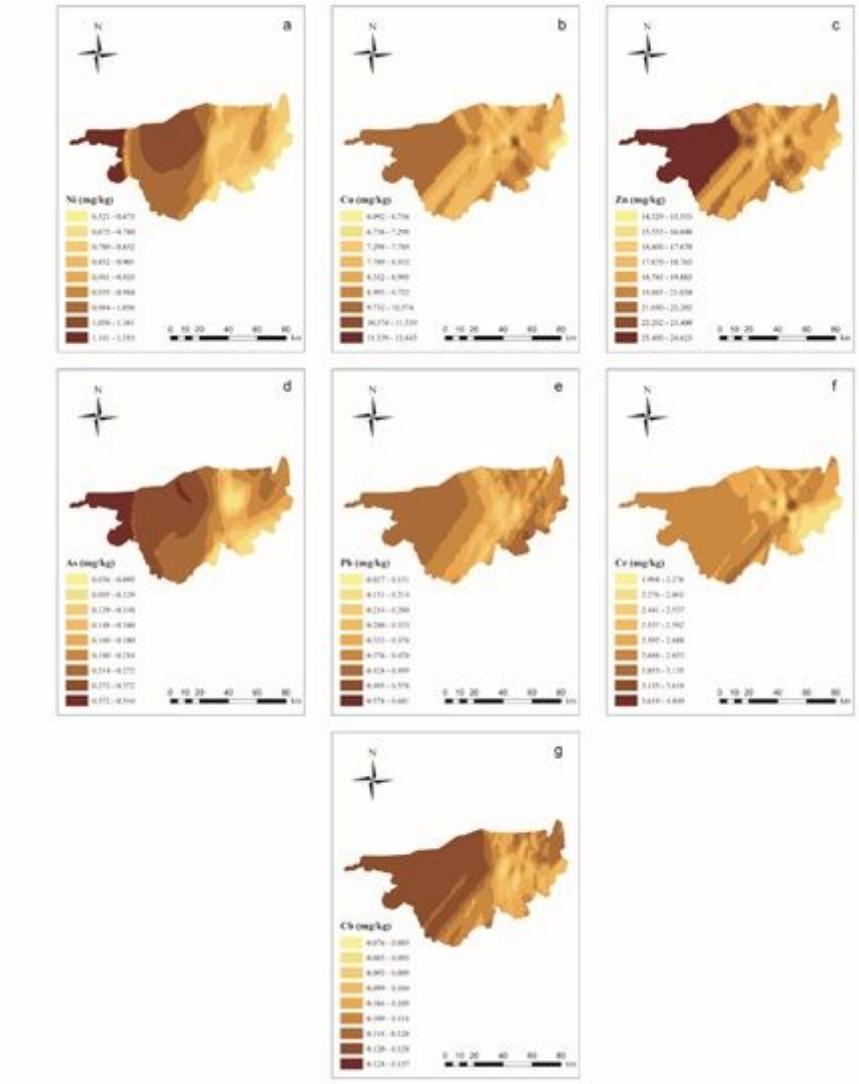

Figure 4

Ordinary Kriging prediction chart of wolfberry PTEs content in the study area (ArcGIS 10.0) Note: This Figure shows the content of PTEs (based on the soil) in the wolfberry of the study area. Different colors represent different contents. Each graph represents different PTEs, a: Ni, b: Cu, c: Zn, d: As, e: Pb, f: Cr, g: Cd. ArcGIS Desktop 10 software with the authorization number of EFL564098460. Note: The designations employed and the presentation of the material on this map do not imply the expression of any opinion whatsoever on the part of Research Square concerning the legal status of any country, territory, city or area or of its authorities, or concerning the delimitation of its frontiers or boundaries. This map has been provided by the authors.

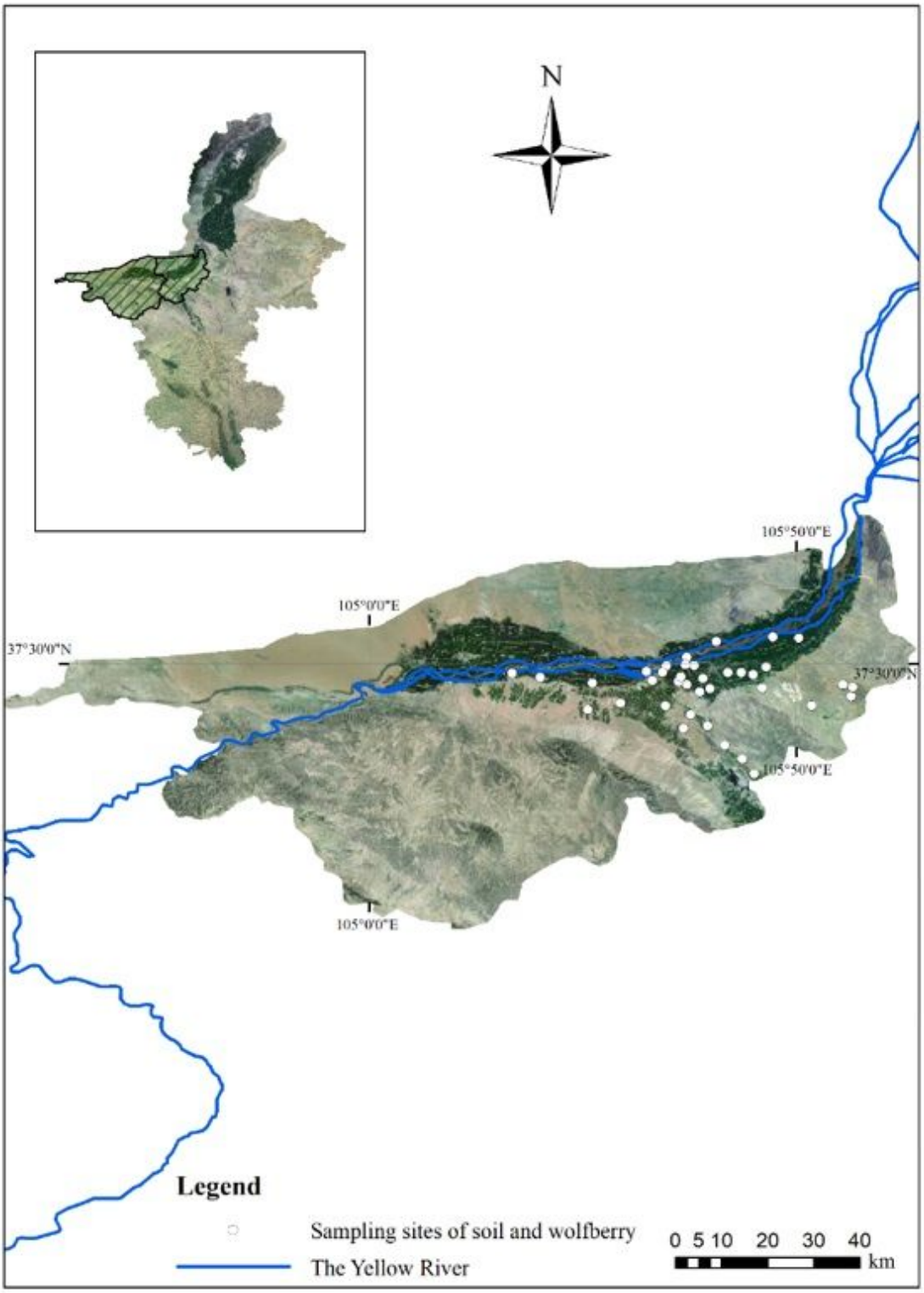

Figure 5

Geomorphology of the study area and sampling sites distribution. Note: The southern part of the study area is mountainous area, the northwest part is desert area, and the dark green area along the Yellow River in the middle part is plain cultivated area. ArcGIS Desktop 10 software with the authorization number of EFL564098460. Note: The designations employed and the presentation of the material on this map do not imply the expression of any opinion whatsoever on the part of Research Square concerning

the legal status of any country, territory, city or area or of its authorities, or concerning the delimitation of its frontiers or boundaries. This map has been provided by the authors.

Supplementary Files

This is a list of supplementary files associated with this preprint. Click to download.

- SupplementaryMaterial.docx